An Acute Increase in TGF beta Increases Permeability of 70 kDa Molecular Tracer from the Heart to Cells Inhabiting Tissue Compartments of the Osteoarthritic Guinea Pig Knee Joint

Lucy Ngo
University of New South Wales
Melissa L. Knothe Tate (proftate.bmwi3@gmail.com)
University of New South Wales

Article

Keywords: molecular transport, drug delivery, cytokines, cells, musculoskeletal system, multimodal imaging, biosystems

Posted Date: June 28th, 2023

DOI: https://doi.org/10.21203/rs.3.rs-3027427/v1

Abstract

A recent pilot study showed that a spike in the inflammatory cytokines TNF-α or TGF-β, delivered via the heart in mature Dunkin-Hartley guinea pigs with osteoarthritis, results in diminished barrier function between the vascular (blood vessels) and respective tissue compartments of bone and muscle [1]. Here we aim to probe effects of TNF-α and TGF-β on barrier function at the vascular interface in different tissue compartments of the knee joint using the same animal model, and with higher resolution imaging modalities including confocal and electron microscopy. First we quantified the intensity of a fluorescent-tagged 70 kDa tracer, similar in size to albumin, the largest transporter protein in the blood, in tissue compartments of bone (periosteum, marrow space, compact bone and epiphyseal bone) and cartilage (articular cartilage, calcified cartilage, and the interface between, i.e. the epiphyseal line), as well as at sites of tendon attachment to bone. We then examined tracer presence and intensity in the respective pericellular and extracellular matrix zones of bone and cartilage. Confirming the previous study, acute exposure to both cytokines reduced barrier function (increased permeability) at vascular interfaces with tissue compartments of the knee joint, with a significant effect in the TGF-β group. Furthermore, this increase in permeability, observed at the length scale of tissue compartments, was also observed at the cellular length scale; the observation of pericellular transport of the albumin-sized molecules to osteocytes contrasts with previous observations of barrier function in healthy, untreated animals and is indicative of reduced barrier function in pericellular regions of cytokine treated animals. The acute, cytokine-induced changes to molecular transport between and within the tissue compartments of the joint, and their respective cellular inhabitants, is of particular relevance for a systems biology understanding of articular joint physiology and interactions between the vascular, musculoskeletal and immune systems, providing impetus for further studies.

1. Introduction

The cellular inhabitants of musculoskeletal tissues rely on patent molecular transport pathways[2] and intact functional barriers[3] to transport between tissues to maintain viability in tissue habitats of intrinsically diverse structure and function. Osteoarthritis (OA), the most common musculoskeletal disorder, is characterized by chronic degeneration of the synovial joints, and is accompanied by pain and disability. While early studies of OA pathogenesis and progression focused on the cartilage degradation, recent research has reconsidered OA as a multifactorial disease affecting all tissues comprising the joint.[4] Similarly, while OA was long-regarded as a non-inflammatory condition, contemporary paradigms recognize the presence of local inflammation in association with and as a major driver of OA progression.[5–7] Concomitant to local inflammation, age-related low-grade systemic inflammation is linked to OA and has been identified as playing a key role in OA's pathogenesis.[8] OA patients exhibit elevated levels of serum inflammatory cytokines.[9] Two such cytokines, TNF-α and TGF-β, have been implicated as inflammatory mediators of OA and are thought to have a critical role in progression of OA.[5,9–11]

Cytokines regulate immune cell function and differentiation and their "dysregulation" is "associated with various human diseases".[12] Cytokines TNF-α and TGF-β are involved in immune regulation and inflammatory responses and have been shown to exhibit both synergistic and antagonistic effects.[13] TNF-α has been shown to increase intestinal permeability (reduce barrier function) by increasing intestinal epithelial tight junction permeability.[14] In contrast, TGF-β has been shown to reduce changes in tight junction proteins induced by TNF-α.[13] Compromise to intestinal barrier function via increased permeability has been identified as "an important pathogenic factor contributing to the development of intestinal inflammation".[14] The role of barrier function and inflammation in osteoarthritis is poorly understood.

The interfaces between the cardiovascular and musculoskeletal system are vital to the maintenance of cellular and joint tissue health, and serve as the gateway for nutrition, waste removal and the delivery of regulatory factors to cells within the musculoskeletal system.[2] These vascular and extravascular pathways allow molecular transport to and between tissues and their cellular inhabitants.[2] It has been shown that the tissues of the joint exhibit the functional barrier property of molecular size and charge selectivity, with changes to permeability with age and/or disease state.[1,15–18] As noted above, the dynamics of the blood-to-tissue barrier function have been shown to be modulated by TNF-α and TGF-β across numerous tissues with underpinning mechanisms related to alteration in tight junction structure and function, and thereby permeability.[14,19–22]

While many studies have focused molecular transport in cartilage and at the osteo-chondral junction, few have examined the multitude of other tissue interfaces that exist within the joint, or their intersection with the cardiovascular system, or how they may be modulated by immune events. Studies from our group over one decade ago demonstrated that ovine periosteum, the sheath bounding all non-cartilaginous outer surfaces of bone, expresses tight junction protein ZO-1.[3,22] Flow resistance studies of ovine femur periosteum permeability indicate a direction and flow rate dependence of permeability, where periosteum is more than twice as permeable in the bone to muscle compared to the opposite direction (Fig. 1A).[3] A more recent study from our group showed that a spike in the inflammatory cytokines TNF-α or TGF-β, delivered via the heart in mature Dunkin-Hartley guinea pigs with osteoarthritis, diminishes barrier function (increased permeability) at the interface of the vascular and bone tissue compartments compared to the untreated baseline control animals (Fig. 1B)[1]. The study compared fluorescence intensity of a fluorescent tagged, 70 kDa dextran, chosen as an inert surrogate for albumin, the 67 kDa, most prevalent transporter protein in the blood. The intensity (directly proportional to concentration[23]) of the fluorescent tagged dextran was measured using cryo-episcopic fluorescent imaging, at near single cell resolution (10.2 × 10.2 μm in plane resolution).[1] Reduction in barrier function was significant for the pro-inflammatory cytokine TGF-β group. These observations of changes to barrier functon provided the impetus for the current study of bone and cartilage compartments within the knee joint of osteoarthritic guinea pig knees exposed to a spike in TNF-α or TGF-β, using higher resolution imaging modalities

(confocal and electron microscopy) after injection of a fluorescent-tagged, fixable dextran, fixation and embedding in plastic resin.

Our overarching hypothesis was that acute increases in OA-associated inflammatory cytokines differentially decrease the barrier function of vascular tissue interfaces within the osteoarthritic joint. Our approach was to investigate the immediate effect of acute increases in inflammatory cytokines on barrier function of vascular tissue interfaces within the tissue compartments of the OA joint, and in the pericellular and extracellular zones of bone and cartilage of the guinea pig knee joint.

2. Results

Immediate Cytokine Modulated Transport within the Joint: After an acute increase in the pro-inflammatory cytokine TNF-α or the anti-inflammatory cytokine TGF-β, no significant differences in tracer concentration could be observed between respective tissue compartments, including blood vessels, bone attachment sites, periosteum, compact bone, epiphyseal bone, marrow/medullary space, epiphyseal line, calcified cartilage, or articular cartilage - neither within nor between the respective compartments of the TNF-α and/or TGF-β groups (Fig. 2). The vascular spaces of the TNF-α group exhibited a mean intensity of 210.5 ± 22.6, ranging from 167.4 to 243.8. The vasculature of the TGF-β group showed a slightly lower mean intensity of 192.5 ± 63.5, with a larger range (71.1 to 285.6, or 2.8 times that of the TNF-α group) in tracer intensity.

In general, the functional barrier between the vasculature and the respective tissue compartments of the knee joint, as measured by the difference in the mean concentration between the two, was significantly diminished in the TGF-β group. For the TNF-α groups, a significant difference in mean tracer intensity was observed between the vasculature and all tissue compartments except the marrow space, indicative of a functional barrier between the vasculature and all respective tissue compartments except the marrow space. The TGF-β group showed fewer significant differences in mean tracer intensity between the vasculature and respective tissue compartments (Fig. 2), indicative of diminished barrier function.

Molecular Transport from the Heart to the Cellular Inhabitants of the Musculoskeletal System: To better understand the spatial distribution of the fluorescent tracer, a heat map depiction of tracer intensity, with warm colors marking areas of high tracer concentration and cool colors showing low tracer concentration, was overlaid onto the stitched confocal images of the joint surface in the saggital plane. The spatial heterogeneity of tracer distribution was grossly observable; the spatial separation of “hot” and “cool spots” generally aligns within the boundaries of tissue compartments. from the articular cartilage to the epiphyseal line of the distal knee (**Supplementary Figure**).

Correlation of relevant anatomical and physiological features in high resolution, stitched (tiled) confocal microscopy images (40x and 63x) and backscattered electron microscopy images (100–1000x) was used to visualize structural and functional properties within and at interfaces between tissue compartments. Following vascular pathways from the heart to the respective tissue compartments of the knee, highest concentrations of the 70 kDa molecular tracer were observed as intense red fluorescence in

the popliteal artery and vein, and to a lesser degree in the marrow space (Fig. 3A). The marrow space showed regions of high tracer concentration; the tracer appeared granular and clustered around the dark adipose cells (Fig. 3B, D). Muscle tissues exhibited diffuse, low levels of tracer, with bone exhibiting even lower levels of tracer compared to muscle. The synovial fluid was devoid of tracer (Fig. 3A).

Within the specific tissue compartments of bone and cartilage, differences in pericellular and extracellular transport were observed in association with acute exposure to inflammatory cytokines. Within bone tissue of the TNF-α and the TGF-β groups, elevated levels of tracer were observed within osteocyte lacunae, within the pericellular matrix (PCM) and surrounding canaliculi. Within the osteocyte itself, tracer was observed concentrated in the perinuclear area where the exosomes are located (Fig. 3B-E), indicative of endocytic transport.

In cartilage tissue of both the TNF-α and TGF-β groups the calcified cartilage exhibited higher intensities of tracer than the underlying bone and capping articular cartilage, increasing with proximity to the articular cartilage; higher concentrations of tracer were present at the boundaries of hypertrophic chondrocytes. Both the TNF-α and TGF-β groups exhibited small amounts of diffuse tracer in the articular cartilage matrix with higher levels of tracer at the cartilage surface. With respect to the cartilage, we observed qualitatively less tracer in the pericellular matrix (PCM), which appeared darker than the surrounding extracellular matrix (ECM). However, no statistically significance was seen in mean tracer intensities between PCM and ECM in cartilage tissue or between the TNF-α and TGF-β groups (Fig. 3F).

Qualitative observations of the TNF-α samples revealed little to no tracer in the PCM in all regions of the cartilage (Fig. 3F). In contrast, animals in the TGF-β group displayed raised levels of tracer within the chondron (PCM), in comparison to the surrounding ECM. Also observed were accumulations of tracer at the tidemark in the TGF-β group, which were not present in the TNF-α group (Fig. 3G).

Based on high resolution confocal microscopy images, the cartilage surfaces of all animals appeared largely intact with some areas exhibiting small amounts of superficial fibrillation; no duplication of the tidemark was detected. The calcified cartilage exhibits slightly increased levels of autofluorescence compared to surrounding articular cartilage and subchondral bone. We observed increased levels of tracer sporadically in osteocytes within the subchondral bone; in addition, the TGF-β group exhibited elevated levels of tracer in some chondrocytes. In some animals, the marrow space appeared to extend through the subchondral bone and the calcified cartilage appeared to merge into the articular cartilage, with the tidemark less apparent at this junction (Fig. 4A).

Subsequent correlative SEM images of the same region of interest showed deterioration of the cartilage surface (Fig. 4B). These areas were observed in confocal images (Fig. 4A). In the SEM images, some areas appearing white, indicative of a change in cartilage composition (increased mineralization) compared to adjoining surface regions (Fig. 4B). Referencing the overview image of this region of interest (Fig. 4A, dotted square), the area of cartilage degeneration is at the metaphysis, near the epiphyseal plate. The boundaries of calcified cartilage are more apparent in SEM images; however, the tidemark is not visible. The images reveal small vessels containing red blood cells within the open connection between

the marrow space and articular cartilage; these were not discernable in the confocal images of the same region of interest (Fig. 4A, B).

3. Discussion

Exposure to a sudden increase in inflammatory cytokines TNF-α and TGF-β changes barrier function at interfaces between the vascular system and the respective tissue compartments making up the osteoarthritic knee joint. Based on the results of this multimodal, multiscale and correlative imaging study, TGF-β exposure diminishes barrier function significantly more compared to TNF-α exposure, which may reflect differences in dosage or respective differences in the effects of pro- and anti-inflammatory cytokines on barrier function. These data implicate the capacity of acute events, such as trauma and cytokine storms induced by viral disease, to significantly impair barrier function between tissues and thereby molecular trafficking, even in osteoarthritic synovial joints which would be exposed to chronic inflammation. Further, the study implicated cytokine induced changes to pericellular and extracellular transport of the large molecular tracer (70 kDa) that mimics transport of albumin (67 kDa), the main carrier protein in the blood plasma. Exposure to both cytokines appeared to increase transport of the large molecular weight tracer to the pericellular region of chondrocytes (the chondron), which may offer a means to open transport pathways for concurrent delivery of pharmaceutical agents that improve chondrocyte viability as well as matrix regeneration by chondrocytes to enable cartilage repair in OA patients.[24] As a whole, the study provides new insights into pathways of transport between the cardiovascular system and the cellular inhabitants of the musculoskeletal system. From a methodological and mechanistic perspective, the study underscores the power of correlative imaging to enable an integrated understanding of complex biosystems and their cellular inhabitants.

The multimodal, correlative imaging across length scales enabled seamless linking of loss in structure and function in OA, from subcellular to organ system length scales. This was particularly apparent with respect to transport of the fluorescent tracer that tracked large molecule traffic from the heart to the cells populating the respective tissues of the synovial joint (Fig. 3–5); akin to tracking truck traffic in road transport networks, future imaging modalities may enable real time assessment of traffic dynamics which would be invaluable for understanding mechanisms of pathophysiology, novel drug delivery strategies, and new preventative health measures.[16,25–28] The current study highlights the near instantaneous nature of the circulation to the joint, with the dextran perfusing all musculoskeletal tissues within the five minute circulation period of the study. The integrated, correlative and multimodal imaging approach also remarkably enabled connection of articular surface degeneration at smallest length scales to mesoscopic biomechanical considerations of joint structure and function, where compositional changes of the surface observed with electron microscopy could be tied to the metaphysis of the joint, where stress concentrations would occur during physiological loading (Fig. 4,5A). All knee joints studied showed cartilage surface fibrillation, marrow space openings into the articular cartilage, and vascular invasion into the articular cartilage, with no tidemark duplication at the osteochondral interface; these all represent morphological features characteristic of early to mild osteoarthritis.[27,29]

A limitation and strength of the study is that the Dunkin-Hartley guinea pigs naturally develop osteoarthritis with age, which precludes study of age-matched controls without OA yet provides a relevant model for the human condition, where onset of OA correlates with age.[15] Use of younger animals prior to onset of OA would not provide an appropriate, independent control, since our previous studies using the same animal model, including a younger cohort, demonstrate an age as well as a disease state dependence on distribution and intensity of fluorescence tracers.[15]

Another recent study from our group, implementing episcopic cryoimaging, showed that exposure to an acute spike of inflammatory cytokine TGF-β significantly reduced vascular barrier function in bone and muscle compared to age-matched controls.[1] This observation provided the impetus for the current study, where plastic embedding and multimodal, higher resolution imaging modalities allowed for quantitative assessment of barrier function in different tissue compartments of the knee joint. For that reason the study design compared tracer transport in two age matched cohorts of the same species with similar stages of OA, where one group was administered a pro-inflammatory cytokine TNF-α and the other was administered an anti-inflammatory cytokine TGF-β.

The study design emulates those carried out to probe the blood-brain barrier and other tissue barrier functions in human patients and animal models.[19–22,30–32] For example, an increase in vascular albumin permeability was reported with exogenously administered TNF-α in *in vivo* mouse model studies of lung, liver, kidney, brain, sciatic nerve, retina, duodenum, jejunum, cecum, thoracic aorta, skin and diaphragm.[33] In contrast to the current acute study observing changes 5 minutes after TNF-α delivery, significant increases were not observed in the mouse study until 12–18 hours after delivery of TNF-α. Furthermore, the published mouse study administered TNF-α at 20 ng/g,[33] a greater than thirty-fold increase in dose compared to the current study. These differences may also reflect intrinsic differences between the healthy murine model and the natural model of OA in the guinea pig. A limitation of the current study is that it was not possible to carry out a dose-response analysis of each cytokine studied due to resource contraints, both with regard to the animal model as well as access to chemical agents (cytokines). The current study, however, provides new insights to guide future investigations and published reports of serum cytokine levels in healthy and diseased, as well as young and aged human cohorts,[1,3,12–14] are also increasing; these will also provide new foundations for future studies.

We observed compartmentalization of molecular transport within the joint similar to that reported in previous studies, and the significant changes in barrier function with exposure to TGF-β confirm those reported in previous cryo-imaging studies,[1,15] irrespective of intrinsic differences in the technologies used for fluorescent imaging of episcopic specimens and laser scanning confocal microscopy (LSCM) imaging. LSCM in general allows for more precise and powerful excitation of fluorophores and capture of emitted light in targeted wavelengths. Further, differences between cryo- and chemically fixed tissues are expected to be minimal, since the cryofixed specimens are fixed and frozen using liquid nitrogen and OCT compared to the chemical fixation of lysine-fixable dextrans for multimodal imaging. Cryofixation occurs

at such low temperatures that any potential diffusive processes are expected to be slowed, and chemical fixation of the “fixable dextrans” containing a primary amine chemically fixes the dextrans in place.[34–36]

Previous experiments have demonstrated the molecular sieving properties of bone where diffusivity decreases with increasing molecular size; at 70 kDa, or *circa* 7 nm Stokes diameter, molecules are no longer able to pass through the bone lacunocanalicular system (LCS).[2,17,37,38] Molecules of molecular weight in the range of TNF-α (17 kDa) and TGF-β (25 kDa) have been reported to permeate the lacunocanalicular system and may modulate barrier properties within the LCS. Here we observed the 70 kDa molecule in the LCS which contradicts previously reports that molecules of this size are excluded from the LCS, even with the aid of mechanical stimuli and associated convective transport.[2,17,39] The circulation time of the tracer in the current study was chosen to match that of previous studies tracing transport from the vascular system to the osteocytes in healthy and acute fracture rodent models; sample sizes also matched those of previous studies.[2,17,18,39,40] Taken together, the current study suggests that the chronic OA disease state, combined with acute exposure to inflammatory cytokines TNF-α and TGF-β, increases LCS permeability and associated transport to osteocytes.

Similarly, the permeability of large molecules in cartilage has been shown to be largely dependent on cartilage composition, which itself depends on health or disease state.[41] It has been demonstrated that changes brought on by OA, i.e. cartilage degradation, also alter tissue structure and composition.[42] In the current study we observed a small amount of tracer within the articular cartilage, with elevated levels of 70 kDa tracer observed inwards toward the articular surface. This suggests that a greater permeability to macromolecules in the cartilage in the middle and deep zones is accompanied by decreased retention in the tissue. This is consistent with findings that different sized antibodies, *e.g.* 25 kDa, 50 kDa, 150 kDa and 200 kDa in size, diffuse into the cartilage with greatest concentrations observed at the articular surface.[43] The diffusion characteristics of 70 kDa dextrans in cartilage PCM have been shown to change with disease state in a porcine model, where healthy animals exhibit significant differences in PCM and ECM diffusion coefficients, and OA animals do not.[44] This is also consistent with our findings that the differences in tracer levels in ECM and PCM were not significant in the guinea pigs which spontaneously develop OA with age. However, the accumulations in the chondron in TGF-β animals but not TNF-α animals suggest that TGF-β may differentially change permeability characteristics of articular cartilage, providing impetus for further studies.

A comparison of tissue compartments between and across the TNF-α and TGF-β groups, did not demonstrate significant differences in bulk permeability of respective tissue compartments. However, the data did show that there was a significant modulation of transport between the bone microvasculature and other tissue compartments in the femur, in the respective groups. Although these cytokines may not necessarily modify the tight junctions at tissue compartment boundaries, they do alter the function of the microvasculature within the joint. TGF-β has been shown to be vital to endothelial barrier function and thus maintenance of microvasculature, with an increase in TGF-β being implicated with the breakdown of the functional tissue barrier at the blood-retinal boundary.[30,31] Similarly, TNF-α has been shown induce

increased vascular permeability through endothelial dysfunction in the brain and lung.[31,32] There is mounting evidence of the association of vascular pathology and OA pathogenesis.[45,46] TNF-α and TGF-β were shown to have an immediate effect on vasculature, and it is hypothesized that cycles of intermittent increase in pro-inflammatory cytokines associated with age-related chronic inflammation may cause further deterioration of the functional barrier at vascular interfaces and may be a contributing factor to OA pathogenesis.

The investigation into transport of macromolecules to and between the compartments of the joint, via the circulatory system through to interstitial transport requires imaging modalities and specimen preparation which allow visualization across multiple length scales, from molecular, cellular, tissue and to organ, e.g. such as the methodologies described here. The current study was not without limitation, as imaging in a single plane (comprising thousands of images) and at a single timepoint captures "a snapshot" during a dynamic process. An ideal imaging modality would also allow for temporal assessment in real time. *In vivo* imaging, albeit currently available at much lower resolution, may provide an additional degree of temporal fidelity; imaging modalities and respective computational capacity are constantly increasing in resolution and speed.

Furthermore, while the molecular weight of the dextran is comparable to that of albumin, dextrans differ both in shape and molecular charge to globular proteins; these factors can affect the mobility of large molecules within tissues. Also, although we observed changes in barrier function between the two groups, in this present study it is not possible to separate the immediate effects of inflammatory cytokines and the chronic effects of exposure to inflammatory cytokines in osteoarthritic, age matched subjects.

4. Conclusion

This study provides further evidence inflammatory cytokines' role in OA pathogenesis, revealing inflammation-induced changes to barrier properties between vascular and tissue compartments of joints exposed to TGF-β. As a whole, these data provide further evidence relating changes in bone-cartilage crosstalk to pathogenesis of osteoarthritis.[46] The study opens new avenues to harness effects of cytokine-driven transport to musculoskeletal tissues for drug delivery.[16,47] The interplay between mechanical loading induced active transport, [2,17,26,39,40,43] mechanoadaptation,[39,48,49] and systemic inflammation[1,18] remains unknown and provides impetus for further study.

5. Experimental Section/Methods

Animal and Surgical Preparation: This study was conducted in accordance with ARRIVE guidelines and regulations. All methods were conducted in accordance with the relevant guidelines and regulations. The study was approved by the Institutional Animal Care and Use Committee (IACUC) at Case Western University (Protocol #2012 – 0100). Six male Dunkin-Hartley guinea pigs, 11–13 months of age (Charles River) were anesthetized via isoflurane and subsequently slowly injected, via the heart, with a single bolus of 70 kDa Texas-red tagged dextrans (Life Technologies, Carlsbad) and either TNF-α (R and D Systems,

Minneapolis, MN) or TGF-β1 (R and D Systems, Minneapolis, MN). The fluorescent tracer was prepared and delivered at a concentration of 1 μg/g body weight, according to previously described protocols.[1,2,15,17,18,39,40,50] TNF-α or TGF-β were dissolved in 0.9% sterile saline solution resulting in dosages of 0.66 ng/g (TNF-α) and 3.33 (TGF-β) ng/g body weight. After five minutes' circulation time post-injection (during which guinea pigs remained anesthetized), animals were euthanized. The circulation time period was chosen to match previous studies in guinea pigs[1] and rodents.[1,2,15,17,18,39,40,50] Immediately after 5 minutes' circulation of the tracer, the knees joints were resected, with care taken to maintain the integrity of the joint including periarticular musculature.

Tissue Embedding: Hindlimbs were prepared *en bloc* for imaging as previously described.[27] Following immersion fixation in 4% paraformaldehyde at 4°C, the specimens were dehydrated via ethanol sequence for polymethylmethacrylate (PMMA) embedding. Once embedded, the specimens were sectioned to expose the tibial-femoral (knee) joint. The joint surface was precision milled in a CNC-lathe, to ensure planarity of the specimen, and polished to a mirror-like finish.

Confocal Laser Scanning Microscopy: Confocal laser scanning microscopy was performed on the specimens using a Zeiss LSM 880 equipped with a 20× 0.8 Plan-Apochromat dry objective and 63× 1.4 Plan-Apochromat oil objective at excitation and emission wavelengths to observe tissue autofluorescence and the Texas-red fluorophore. The resulting 5000 + images per block face were stitched and rendered, creating navigable maps, using the Google Maps API per methods previously developed for the visualization and analysis of electron microscopy of human-sized joints.[26–28, 48,50,51] For quantification of tracer permeability, the images were scaled down by a factor of 0.25 using Arivis Vision4D (Arivis AG, Germany) and exported to TIF format. Tissue compartments in the region distal to and including the epiphyseal plate – articular cartilage, calcified, bone, marrow, the epiphyseal plate, epiphyseal bone, periosteum, bone microvasculature and tendon or ligament attachment sites – were manually segmented in Fiji (Fiji Is Just ImageJ). Heatmaps of tracer density were computed using Matlab (MathWorks Inc., Natick, MA).

Backscattered Electron Scanning Electron Microscopy: To further decipher the interactions of the tracer with musculoskeletal tissue and cells, the specimens were stained with iodine and potassium iodine to enhance the contrast of cellular and soft tissue components according to published protocols.[50,51] The specimens then underwent backscattered electron scanning electron microscopy performed on a FEI NanoSEM 450.

Statistical Analysis: Two-way ANOVA statistical analysis and Sidak's multiple comparisons *post hoc* analysis was performed for comparisons of tracer across groups and between multiple tissue compartments. $p < 0.05$ was considered significant; means and standard errors are reported. All statistical analysis was performed using GraphPad Prism 8 (GraphPad Software, San Diego California USA).

Declarations

Acknowledgements

Supported in part through the National Health and Medical Research Council, the Paul Trainor Foundation, and the Blue Mountains World Interdisciplinary Innovation Institute. We would also like to acknowledge the scientific and technical assistance, as well as the facilities of Dr. Judith Drazba and the Lerner Research Institute Core Facilities at Cleveland Clinic, Microscopy Australia at the Electron Microscope Unit (EMU), and the Biomedical Imaging Facility (BMIF), now called the Katharina Gaus Imaging Facility to honor the late Professor Gaus, within the Mark Wainwright Analytical Centre (MWAC) at UNSW Sydney.

Data availability

The datasets generated and/or analysed during the current study are available in the MechBio data repository, on the Blue Mountains World Interdisciplinary Institute website https://mechbio.org or https://blueinnovations.org, under the section "Data Repositories". In addition, the datasets used and/or analysed during the current study are available from the corresponding author on reasonable request.

References

1. L. Ngo, M.L. Knothe Tate (2023) A spike in circulating inflammatory cytokines alters barrier function between vascular and musculoskeletal tissues, Nature Sci Reports, 9119, https://doi.org/10.1038/s41598-023-30322-7
2. M.L. Knothe Tate, P. Niederer, U. R. Knothe (1998) In vivo tracer transport through the lacunocanalicular system of rat bone in an environment devoid of mechanical loading, Bone 22, 107–17.
3. S. Evans, J. Parent, C. Lasko, X. Zheng, U. Knothe, T. Lemaire, M.L. Knothe Tate (2013) Periosteum, Bone's "Smart" Bounding Membrane, Exhibits Direction Dependent Permeability, Journal of Bone and Mineral Research 28(3): 608–17.
4. R. F. Loeser, S. R. Goldring, C. R. Scanzello, M. B. Goldring (2012) Osteoarthritis: a disease of the joint as an organ, Arthritis Rheum. 64, 1697–1707.
5. J. Sokolove, C. M. Lepus (2013) Role of inflammation in the pathogenesis of osteoarthritis, Ther. Adv. Musculoskelet. Dis. 5, 77–94.
6. M. Rahmati, A. Mobasheri, M. Mozafari (2016) Inflammatory mediators in osteoarthritis: a critical review of the state-of-the-art, current prospects, and future challenges, Bone 85, 81–90.
7. F. Berenbaum (2013) Osteoarthritis as an inflammatory disease, Osteoarthr. Cartil. 21, 16–21.
8. A.M. Malfait (2016) Osteoarthritis year in review 2015: Biology, Osteoarthr. Cartil. 24, 21–26 (2016).
9. E. Rezuș, A. Cardoneanu, A. Burlui, A. Luca, C. Codreanu, B. Tamba, G.-D. Stanciu, N. Dima, C. Bădescu, C. Rezuș (2019) The link between inflammaging and degenerative joint diseases, Int. J.

Mol. Sci. 20, 614.

10. J. F. Muñoz-Valle, E. Oregón-Romero, H. Rangel-Villalobos, G. E. Martínez-Bonilla, E. Castañeda-Saucedo, L. Salgado-Goytia, M. A. Leyva-Vázquez, B. Illades-Aguiar, L. del C. Alarcón-Romero, M. Espinoza-Rojo, I. Parra-Rojas (2014) High expression of TNF alpha is associated with – 308 and – 238 TNF alpha polymorphisms in knee osteoarthritis. *Clin. Exp. Med.* 2014, *14*, 61–67.
11. P. Wojdasiewicz, L. A. Poniatowski, D. Szukiewicz (2014) The role of inflammatory and anti-inflammatory cytokines in the pathogenesis of osteoarthritis, Mediators Inflamm. 1–19.
12. H.O. Kim, H.S. Kim, J.C. Youn, E.C. Shin, S. Park (2011) Serum cytokine profiles in healthy young and elderly population assessed using multiplexed bead-based immunoassays. J Transl Med. 20(9):113.
13. Z.W. Liu, Y.M. Zhang, L.Y. Zhang, T. Zhou, Y.Y. Li, G.C. Zhou, Z.M. Miao, M. Shang, J.P. He, N. Ding, Y.Q. Liu (2022) Duality of Interactions Between TGF-β and TNF-α During Tumor Formation. Front Immunol. 12:810286.
14. R. Al-Sadi, S. Guo, D. Ye, T.Y. Ma (2013) TNF-α modulation of intestinal epithelial tight junction barrier is regulated by ERK1/2 activation of Elk-1. Am J Pathol. 183(6):1871–1884.
15. L. Ngo, L. E. Knothe, M. L. Knothe Tate (2018) Knee joint tissues effectively separate mixed sized molecules delivered in a single bolus to the heart, Sci. Rep. 8, 10254.
16. L. Ngo, M. L. Knothe Tate (2020) Osteoarthritis: New strategies for transport and drug delivery across length scales, ACS Biomater. Sci. Eng. 6, 6009–6020.
17. A. E. Tami, M. B. Schaffler, M. L. Knothe Tate (2003) Probing the tissue to subcellular level structure underlying bone's molecular sieving function, Biorheology 40, 577–90.
18. A. Tami, P. Nasser, M.B. Schaffler, M.L. Knothet Tate (2003) Non-invasive fatigue fracture model of the rat ulna, Journal Orthopaedic Research, 21(6): 1018–1024.
19. P. R. Clark, R. K. Kim, J. S. Pober, M. S. Kluger (2015) Tumor necrosis factor disrupts Claudin-5 endothelial tight junction barriers in two distinct NF-ï «ï ç-dependent phases, PLoS One 10, e0120075.
20. P. T. Ronaldson, K. M. DeMarco, L. Sanchez-Covarrubias, C. M. Solinsky, T. P. Davis (2009) Transforming growth factor-ï çï signaling alters substrate permeability and tight junction protein expression at the blood-brain barrier during inflammatory pain, *J. Cereb. Blood Flow Metab.* 2009, *29*, 1084–1098.
21. K. L. Howe, C. Reardon, A. Wang, A. Nazli, D. M. McKay (2005) Transforming growth factor-beta regulation of epithelial tight junction proteins enhances barrier function and block enterohemorrhagic Escherichia coli O157:H7-induced increased permeability, *Am. J. Pathol.* 2005, *167*, 1587–97.
22. S. F. Evans, D. Docheva, A. Bernecker, C. Colnot, R. P. Richter, M. L. Knothe Tate (2013) Solid-supported lipid bilayers to drive stem cell fate and tissue architecture using periosteum derived progenitor cells, *Biomaterials* 2013, *34*, 1878–87.
23. K. Lee, E. Shirshin, N. Rovnyagina, F. Yaya, Z. Boujja, A. Priezzhev, & C. Wagner (2018) Dextran adsorption onto red blood cells revisited: Single cell quantification by laser tweezers combined with microfluidics. Biomedical Optics Express 9, 2755 doi:10.1364/BOE.9.002755.

24. O.-M. Aho, M. Finnilä, J. Thevenot, S. Saarakkala, P. Lehenkari (2017) Subchondral bone histology and grading in osteoarthritis, PLoS One 12, e0173726.
25. E. J. Anderson, S. M. Kreuzer, O. Small, M. L. Knothe Tate (2007) Pairing computational and scaled physical models to determine permeability as a measure of communication in micro- and nano-scale pericellular spaces, Microfluidics and Nanofluidics, 4, 193–204.
26. D. Hageman, A. F. Pereira, D. Zeidler, U. R. Knothe, L. Gardner, M. L. Knothe Tate (2016), Cellular Epidemiology of Human Disease using Biogeographic and Google Maps Approaches - Towards Definition of Cell Network Indices for Rapid Diagnostics, *Ann. Biomed. Eng.* 2016, *44*, 3719.
27. M. L. Knothe Tate, D. Zeidler, A. F. Pereira, D. Hageman, T. Garbowski, S. Mishra, L. Gardner, U. R. Knothe (2016) Organ-to-cell-scale health assessment using geographical information system approaches with multibeam scanning electron microscopy, *Adv. Healthc. Mater.* 2016, *5*, 1581–1587.
28. A. F. Pereira, D. J. Hageman, T. Garbowski, C. Riedesel, U. R. Knothe, D. Zeidler, M. L. Knothe Tate (2016) Creating high-resolutio multiscale maps of human tissue using multi-beam SEM, *PLoS Comput. Biol.* 2016, *12*, e1005217.
29. A. Boyde (2012) Staining plastic blocks with triiodide to image cells and soft tissues in backscattered electron SEM of skeletal and dental tissues, Eur. Cells Mater. 24, 154–161.
30. T. E. Walshe, M. Saint-Geniez, A. S. R. Maharaj, E. Sekiyama, A. E. Maldonado, P. A. D'Amore (2009) TGF-beta is required for vascular barrier function, endothelial survival and homeostasis of the adult microvasculature, PLoS One, 4, e5149.
31. M. A. Behzadian, X. L. Wang, L. J. Windsor, N. Ghaly, R. B. Caldwell (2001) TGF-beta increases retinal endothelial cell permeability by increasing MMP-9: possible role of glial cells in endothelial barrier function, Investig. Ophthalmol. Vis. Sci. 42, 853–859.
32. K. S. Mark, D. W. Miller (1999) Increased permeability of primary cultured brain microvessel endothelial cell monolayers following TNF-alpha exposure, Life Sci., 64, 1941–1953.
33. Worrall, N.K., Chang, K., Lejeune, W.S., Misko, T.P., Sullivan, P.M., Ferguson, T.B., & Williamson, J.R. TNF-α causes reversible in vivo systemic vascular barrier dysfunction via NO-dependent and -independent mechanisms. Am. J. Physiol. Circ. Physiol. 273, H2565–H2574 (1997).
34. L. Edelmann (2002) Freeze-dried and resin-embedded biological material is well suited for ultrastructure research, *J. Microsc.* 2002, *207*, 5–26.
35. G. E. Sosinsky, J. Crum, Y. Z. Jones, J. Lanman, B. Smarr, M. Terada, M. E. Martone, T. J. Deerinck, J.E. Johnson, M. H. Ellisman (2008) The combination of chemical fixation procedures with high pressure freezing and freeze substitution preserves highly labile tissue ultrastructure for electron tomography applications, J. Struct. Biol. 161, 359–371.
36. P. R. Pryor (2012) Analyzing lysosomes in live cells, *Methods Enzymol.* 2012, *505*, 145–157.
37. S. Weinbaum, S. C. Cowin, Y. A. Zeng (1994) A model for the excitation of osteocytes by mechanical loading-induced bone fluid shear stresses, J. Biomech. 27, 339–360.
38. L. Wang, C. Ciani, S. B. Doty, S. P. Fritton (2004), Delineating bone's interstitial fluid pathways in vivo, Bone 34, 499–509.

39. M. L. Knothe Tate, R. Steck, M. R. Forwood, P. Niederer (2000) *In vivo* demonstration of load-induced fluid flow in the rat tibia and its potential implications for processes associated with functional adaptation, Journal of Experimental Biology, 203(18): 2737–2745. eid:2-s2.0-0033793551
40. M. L. Knothe Tate, A.E. Tami, P. Netrebko, S. Milz, D. Docheva (2012) Multiscale computational and experimental approaches to elucidate bone and ligament mechanobiology using the ulna-radius-interosseous membrane construct as a model system, *Technol. Heal. Care* 2012, *20*, 363–378.
41. H. A. Leddy, F. Guilak (2003) Site-specific molecular diffusion in articular cartilage measured using fluorescence recovery after photobleaching, *Ann. Biomed. Eng.* 2003, *31*, 753–60.
42. A. Maroudas, M. T. Bayliss, M. F. Venn (1980) Further studies on the composition of human femoral head cartilage, Ann. Rheum. Dis. 39, 514–23.
43. C. D. DiDomenico, A. Goodearl, A. Yarilina, V. Sun, S. Mitra, A. S. Sterman, L. S. Bonassar (2017) The effect of antibody size and mechanical loading on solute diffusion through the articular surface of cartilage, *J. Biomech. Eng.* 2017, *139*.
44. H. A. Leddy, S. E. Christensen, F. Guilak (2008) Microscale diffusion properties of the cartilage pericellular matrix measured using 3D scanning microphotolysis, J. Biomech. Eng., 130.
45. D. M. Findlay (2007) Vascular pathology and osteoarthritis Rheumatology 46, 1763–1768.
46. D. M. Findlay, J. S. Kuliwaba (2016) Bone-cartilage crosstalk: a conversation for understanding osteoarthritis, Bone Res. *4*, 16028.
47. X. L. Yuan, H. Y. Meng, Y. C. Wang, J. Peng, Q. Y. Guo, A. Y. Wang, S. B. Lu (2014) Bone-cartilage interface crosstalk in osteoarthritis: potential pathways and future therapeutic strategies, Osteoarthritis and Cartilage 22, 1077–1089.
48. M.L. Knothe Tate, A. Srikantha, C. Wojek, D. Zeidler (2021) Connectomics of Brain to Bone - Probing Physical Renderings of Cellular Experience, Frontiers in Physiology | Integrative Physiology, 12:647603, doi: 10.3389/fphys.2021.647603.
49. V.L.D. Putra, K. Kilian, M.L. Knothe Tate (2023) Cytoskeletal Remodelling in Tissue Development and Regeneration, Nature Communications Biology, 6(1): 75, doi: 10.1038/s42003-022-04320-w.
50. L. Ngo, A. Nathanson, T. Garbowski, U. R. Knothe, D. Zeidler, M. L. Knothe Tate (2019) Electron microscopy sample preparation protocol enabling nano-to-mesoscopic mapping of cellular connectomes and their habitats in human tissues and organs, *Bio-protocol 9*, e3298.
51. L. Ngo, M. L. Knothe Tate. Multi-Modal Sample Preparation and Imaging Protocol for Nano-to-mesoscopic Mapping of Cellular Inhabitants in Diverse Tissue Compartments, Across Organ Systems, 30 May 2023, PROTOCOL (Version 1) available at Protocol Exchange [https://doi.org/10.21203/rs.3.pex-2244/v1]

Figures

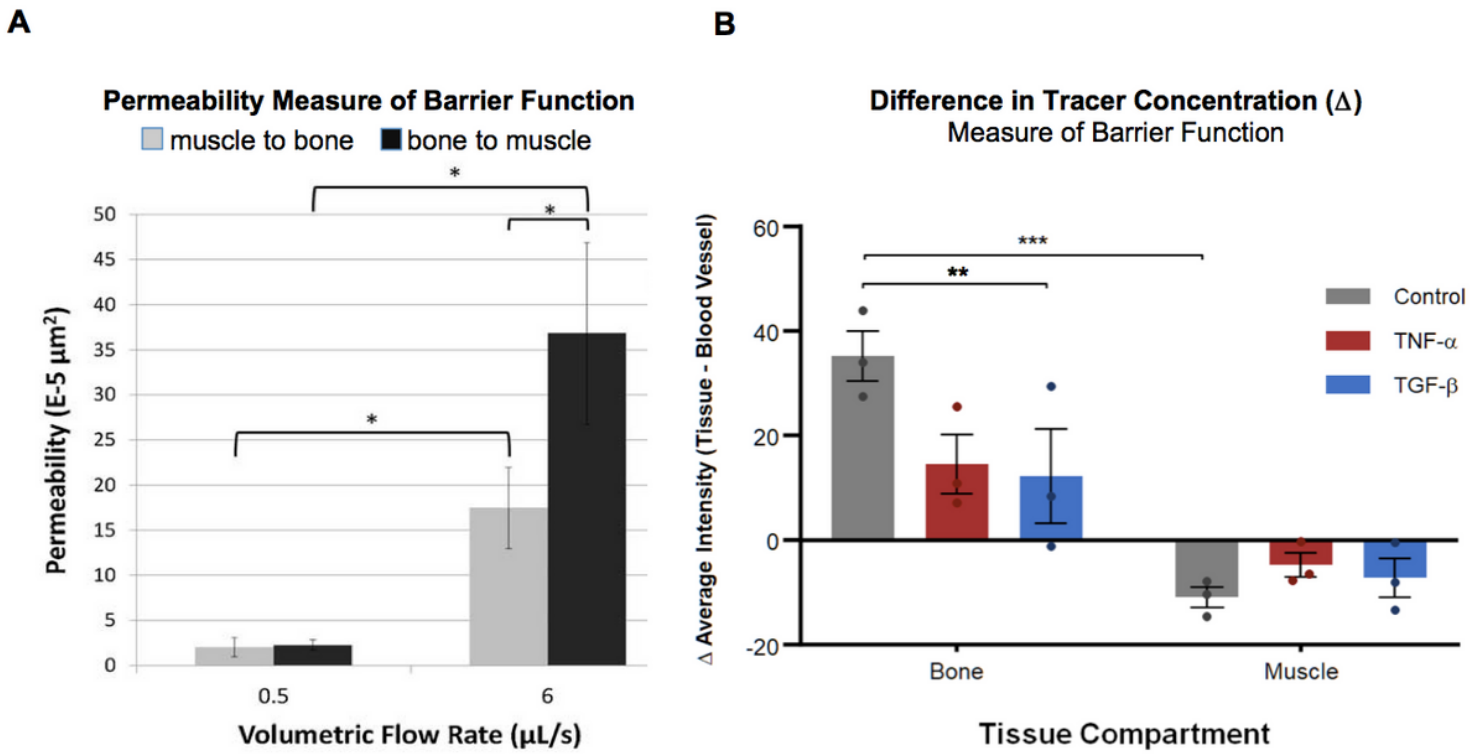

Figure 1

Measures of barrier function in bone, muscle, and periosteum (tissue sheath between bone and muscle). These observations of changes to barrier functon provided the impetus for the current study of bone and cartilage compartments within the knee joint of osteoarthritic guinea pig knees, using higher resolution imaging modalities (confocal and electron microscopy) after injection of a fluorescent-tagged, fixable dextran, fixation and embedding in plastic resin.

A. Periosteum is a sheath bounding all non-cartilaginous outer surfaces of bone. Flow resistance studies of ovine femur periosteum permeability indicate a direction and flow rate dependence of permeability, where periosteum is more than twice as permeable in the bone to muscle compared to the opposite direction. Significance is indicated by *: $p < 0.05$. Figure reproduced with permission.[3]

B. Episcopic cryoimaging data measuring the intensity of fluorescent tracer (a measure of concentration[1]) shows barrier function (difference in concentration of tracer) at vascular interfaces within bone and muscle of guinea pig knee joints. In untreated control tissues, barrier function at vascular interfaces is significantly higher in bone than in muscle (***: $p < 0.001$). In bone, treatment with either cytokine TNF-a or TGF-b reduces barrier function, with a significant reduction in the TGF-b group (**: $p < 0.05$). Figure reproduced with permission.[1]

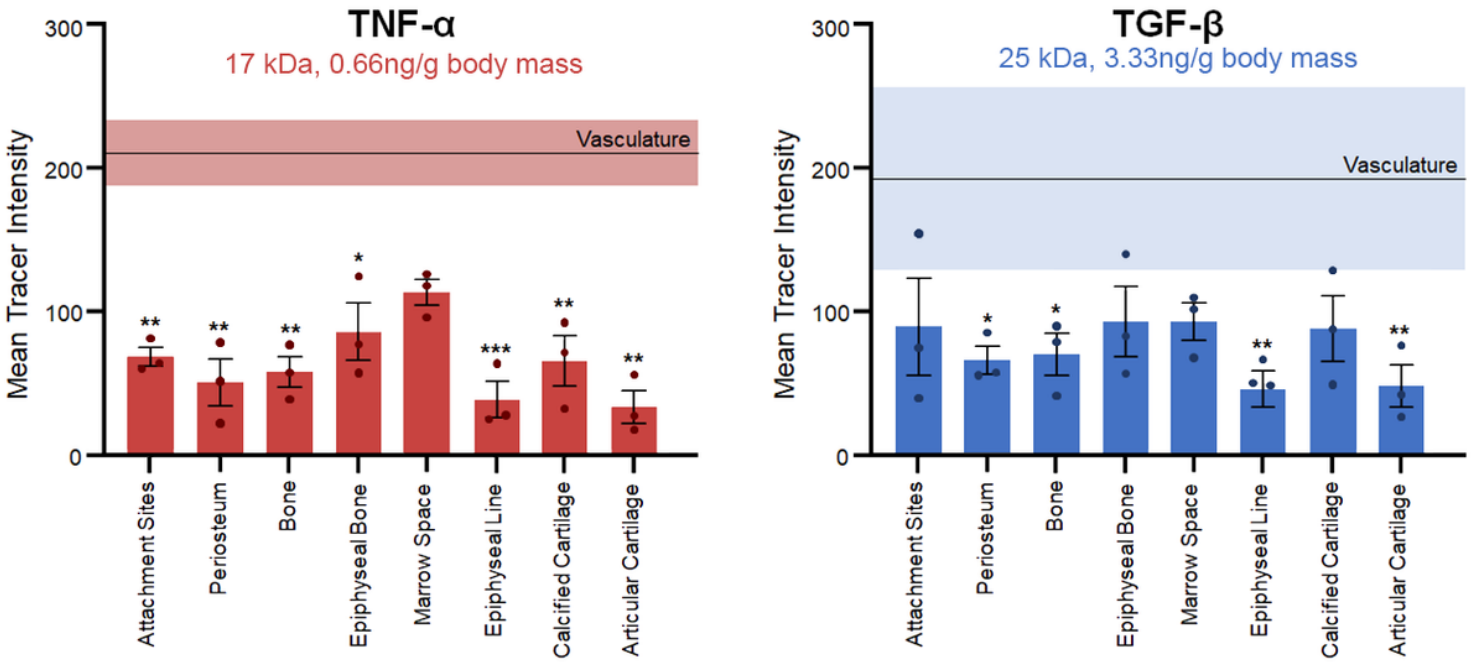

Figure 2

Effect of an acute increase in inflammatory cytokines TNF-α or TGF-β on mean 70 kDa tracer intensity in tissue and vasculature compartments within the joint, showing significant (*,**,***) differences in concentrations between tissues of the knee and the vascular compartment. The shaded horizontal bands indicate the ranges of mean tracer intensity +/- SEM for respective vascular compartments of the TNF-α and TGF-β groups. The mean intravascular tracer intensity tracer is similar between the two groups (around 200) but the range of intensities is much greater in the TGF-β than the TNF-α group. The range of intensities for vascular compartments in TGF-β exposed animals is *circa* 2.8 times that of the respective TNF-α exposed vascular compartments, indicative of loss in barrier function. Providing further evidence for loss in barrier function at the vascular interface of the TGF-b exposed group, fewer significant differences were observed between tracer concentrations in the respective tissues and vascular compartments of the TGF-β than the TNF-α group. Tissue compartments are organized roughly from outside-in and distal to proximal to the articular surface, *i.e.* tendon insertions to bone (Attachment Sites), periosteum covering the outer surface of bone (Periosteum), compact bone (Bone), Epiphyseal Bone, bone marrow/medullary space (Marrow Space), Epiphyseal Line, Calcified Cartilage, Articular Cartilage. Significant differences were determined by two-way ANOVA and Tukey's multiple comparisons post hoc analysis. Error bars indicate standard error ($n = 3$). Statistical significance indicated by *($p < 0.05$), **($p < 0.01$), and ***($p < 0.001$).

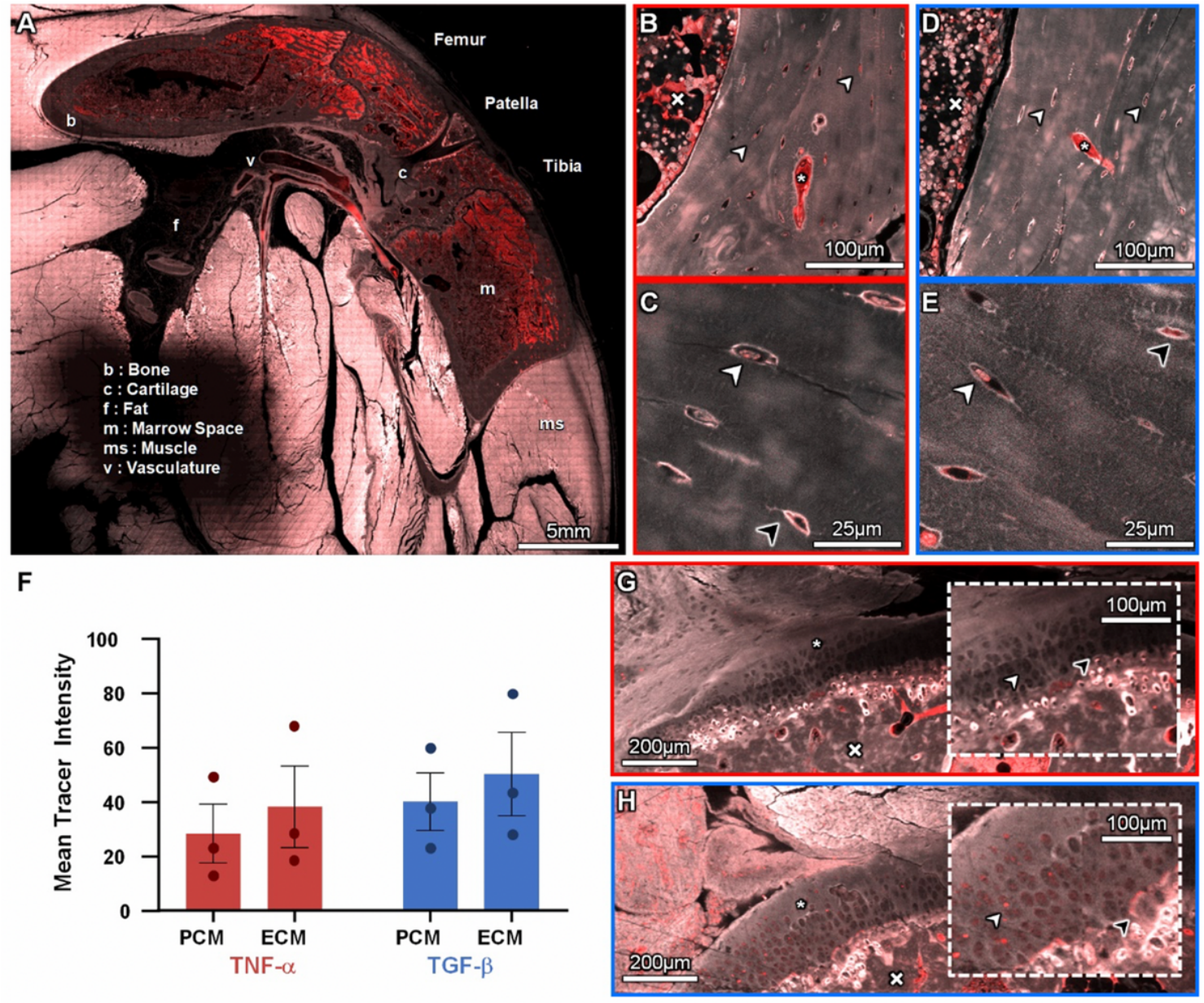

Figure 3

Molecular transport from the heart to the cellular inhabitants of the musculoskeletal system, accounting for presence of the tracer (70 kDa) in PCM and ECM regions. (A) Overview of sagittal cross-section of the knee, showing molecular separation of tracer (red) in autofluorescence musculoskeletal tissues (white), visualized using ~5168 confocal microscopy fields of view. At higher magnification, some regions show tracer within the vasculature and osteocyte lacunae in (B-C) TNF-α and (D-E) TGF-βgroups; crosses denote marrow and asterisks indicate vasculature. Light and dark arrowheads point to tracer within intracellular and/or pericellular regions of osteocytes, respectively. (F) Comparison of mean tracer intensity in the PCM and ECM of cartilage in the TNF-α and TGF-βgroups. No significant differences were noted between cytokine groups or regions of interest (two-way ANOVA and Tukey's multiple comparisons post hoc analysis). (G) TNF-α animals exhibited small amounts of tracer in the ECM, with decreased tracer in the PCM. (H) In TGF-β animals, similar patterns of tracer were observed in the cartilage, except

for elevated tracer levels at the tidemark and within the chondron, neither of which were observed in TNF-α animals. (G,H) Crosses denote subchondral bone, asterisks indicate cartilage, light arrowheads point to chondrons and dark arrowheads point to the tidemark.

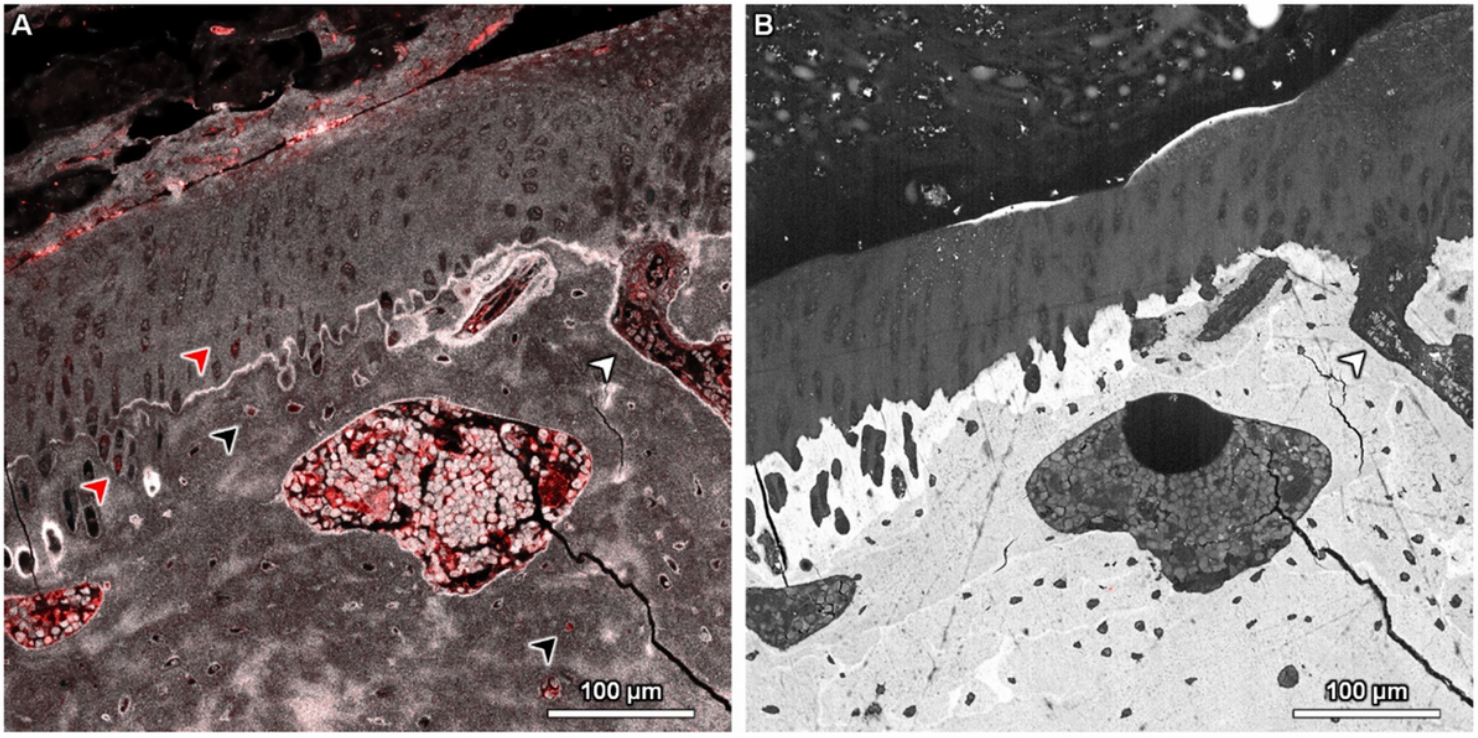

Figure 4

Multimodal imaging of the osteochondral junction – cartilage, subchondral bone, and underlying marrow spaces. White arrow points to marrow space that extends past the subchondral bone and calcified cartilage into the articular cartilage. (A) Confocal microscopy with 70 kDa dextran appearing red and tissue autofluorescence in white. Red and black arrows indicate chondrocytes and osteocytes, respectively, with greater levels of tracer compared to other cells in the region of interest. (B) BS-SEM image of iodine stained and carbon coated specimen showing calcified and non-calcified tissue regions. Calcified cartilage appears brighter than surrounding bone. Red blood cells (indicated by white arrowhead) appear within a vessel in a region of marrow that extends into the articular cartilage. The crack in the lower right corner is an artifact of sample preparation.

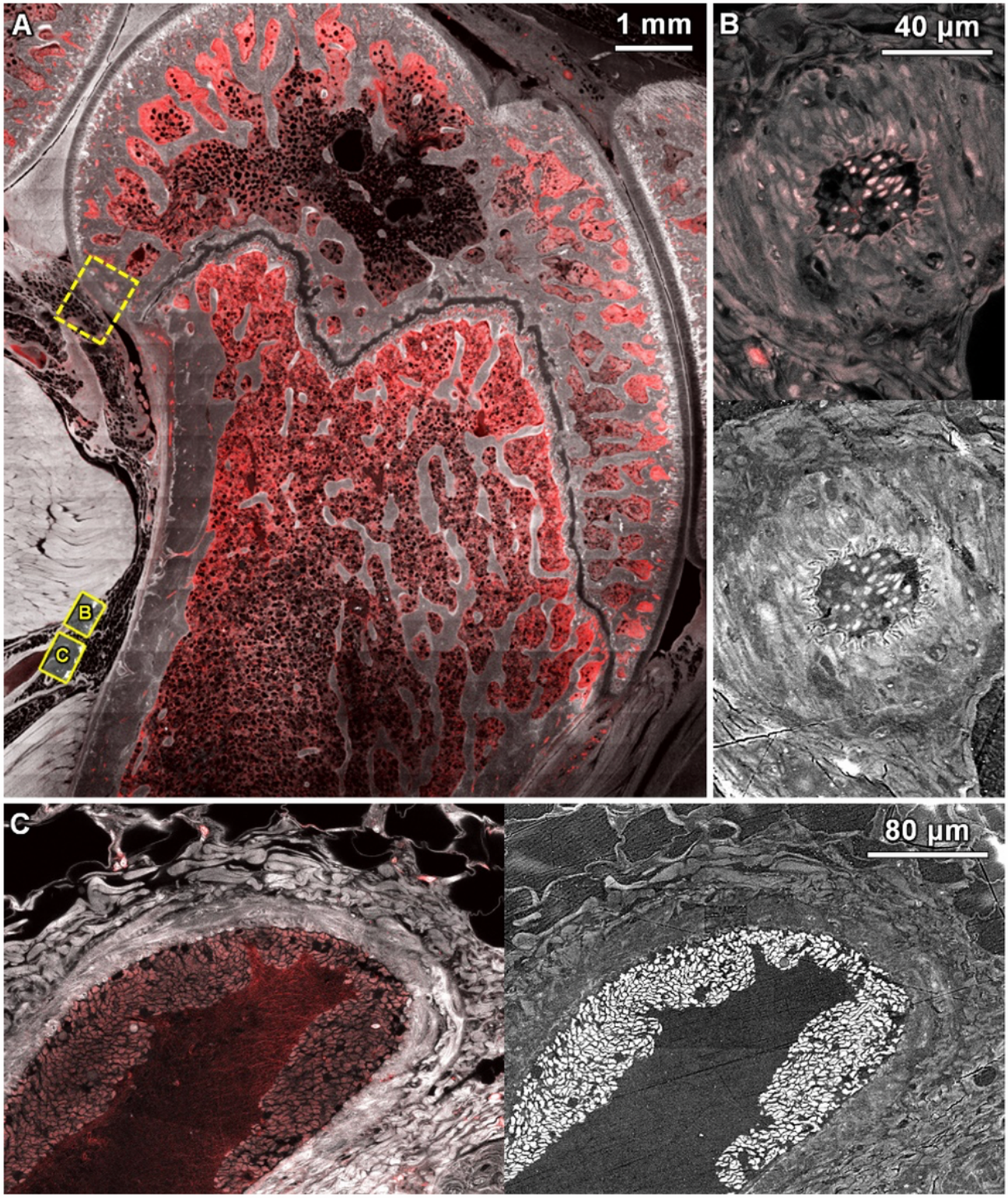

Figure 5

Imaging at the interface of the cardiovascular and musculoskeletal systems demonstrates the power of multiscale, multimodal, and correlative imaging. (A) Multi-modal imaging of the guinea pig distal femur. An overview image of the guinea pig distal femur comprises tiles of confocal microscopy images with overlaid regions of interest acquired with BSE-SEM. The correlated confocal and electron microscopy region of interest from **Figure 4** is depicted by the dashed, yellow square outline. Confocal (B, top and C,

left) and BSE-SEM (C, bottom, and C, right) images depict the popliteal vasculature (B – popliteal artery, C – popliteal vein). Confocal images help in visualizing relationships between the fluid elements of the vascular system (red, 70 kDa tracer), where albumin-sized (67 kDa) molecules would permeate, and the musculoskeletal tissue matrices (PCM as well as the ECM, see **Figure 3**). Electron microscopy highlights cellular inhabitants in the vascular and extravascular tissues and structure-function relationships of the cardiovascular system. Correlative imaging allows concomitant visualization of these elements for any given field of view of interest, from nano to meso-length scales.

Supplementary Files

This is a list of supplementary files associated with this preprint. Click to download.

- 2023SciRep2v3SupplementaryFigure.docx